International Journal of Nanomedicine

Dovepress
open access to scientific and medical research

Open Access Full Text Article

ORIGINAL RESEARCH

Antimicrobial Activity of Graphene Oxide Contributes to Alteration of Key Stress-Related and Membrane Bound Proteins

Vaishnavi Ravikumar[1], Ivan Mijakovic[1,2], Santosh Pandit[2]

[1]Novo Nordisk Foundation Center for Biosustainability, Technical University of Denmark, Kongens Lyngby, Denmark; [2]Department of Biology and Biological Engineering, Chalmers University of Technology, Göteborg, 41296, Sweden

Correspondence: Santosh Pandit, Department of Biology and Biological Engineering, Chalmers University of Technology, Kemivägen 10, Göteborg, 41296, Sweden, Tel +46 729484011, Fax +46 317723801, Email pandit@chalmers.se

Introduction: Antibacterial activity of graphene oxide (GO) has been extensively studied, wherein penetration of the bacterial cell membrane and oxidative stress are considered to play a major role in the bactericidal activity of GO. However, the specific mechanism responsible for the antibacterial activity of GO remains largely unknown. Hence, the goal of this study was to explore the mode of action of GO, via an in-depth proteomic analysis of the targeted bacteria.

Methods: *Staphylococcus aureus* was grown in the presence of GO and samples were collected at different growth phases to examine the cell viability and to analyze the changes in protein expression. Antimicrobial efficiency of GO was tested by assessing bacterial viability, live/dead staining and scanning electron microscopy. The intracellular reactive oxygen species (ROS) induced by GO treatment were examined by fluorescence microscopy. Label-free quantitative proteomics analysis was performed to examine the differentially regulated proteins in *S. aureus* after GO treatment.

Results: GO treatment was observed to reduce *S. aureus* viability, from 50 ± 17% after 4 h, to 93 ± 2% after 24 h. The live/dead staining confirmed this progressive antimicrobial effect of GO. SEM images revealed the wrapping of bacterial cells and their morphological disruption by means of pore formation due to GO insertion. GO treatment was observed to generate intracellular ROS, correlating to the loss of cell viability. The proteomics analysis revealed alteration in the expression of cell membrane, oxidative stress response, general stress response, and virulence-associated proteins in GO-treated bacterial cells. The time-dependent bactericidal activity of GO correlated with a higher number of differentially regulated proteins involved in the above.-mentioned processes.

Conclusion: The obtained results suggest that the time-dependent bactericidal effect of GO is attributed to its wrapping/trapping ability, ROS production and due to physical disruption of the cell membrane.

Keywords: cell wrapping, membrane disruption, oxidative stress, proteomics

Introduction

Graphene oxide is a derivative of graphene, with an oxygen moiety and many other functional groups on its surface, including epoxy, hydroxyl, and carboxyl groups on the monolayer sp^2 -bonded carbon.[1] The presence of the oxygen group makes GO more suitable than pristine graphene for some applications.[2] Due to its hydrophilic nature, GO is highly dispersive in aqueous medium, which provides enormous opportunities for many biological applications, including antimicrobial activity.[3,4] Additionally, other characteristics of GO including ease of synthesis, size tunability, low cytotoxicity and biocompatibility, are attracting immense attention among researchers in the biomedical field. Hence, GO has been utilized not only as an antimicrobial material, but also as a drug carrier for drug delivery, in tissue engineering and in sensors.[5–9] Many studies have demonstrated the broad-spectrum antibacterial potential of GO against various bacterial strains, including phytopathogens and bacterial biofilms.[10–12] This broad-spectrum antimicrobial efficiency of GO was demonstrated using free GO in solution or in the form of surface coatings.[13–16]

Received: 6 September 2022
Accepted: 7 December 2022
Published: 28 December 2022

The bactericidal efficiency of GO is considered to be mediated mainly by the physical and chemical interactions of GO nanosheets with the bacterial cell upon close contact.[17–20] In this regard, damage of the bacterial cell membrane has been shown to occur due to the knife-like edges of the GO nanosheets, which cut through the cell membrane resulting in disruption of the membrane integrity.[15,17–23] Membrane damage or pore formation on the cell membrane has been seen to alter the cell morphology and lead to release of sub-cellular components such as nucleic acids and electrolytes, resulting in alteration of the transmembrane potential.[15,24,25] The bacterial membrane damage is also considered to be mediated by lipid peroxidation, caused by the oxidative effect of GO.[26,27] Hence oxidative stress generated by GO has been proposed as a major contributor for its bactericidal activity. However, either internalization via penetration or charge transfer from the cell membrane to the oxygen functional group of GO may be necessary to induce the ROS.[1,27,28] Reactive oxygen species (ROS) mainly superoxide, hydrogen peroxide and hydroxyl radicals are key elements in the bacterial response to lethal stress. Thus, the contact-mediated bactericidal efficiency of GO has attracted substantial interest for the development of antimicrobial or self-sterilizing surfaces.[15,29–31] In fact, the contact-killing mode could provide significant benefits over metallic nanoparticle coatings which have a disadvantage of releasing toxic metal ions.[32,33] So far, the potential of GO to induce oxidative stress is mostly demonstrated by its efficiency to oxidize glutathione.[24,26,34,35]

The current understanding of the mechanism of action by which GO acts bactericidally revolves (i) around the penetration of the bacterial cell membrane by the sharp edges of the nanosheets, resulting in cell damage, (ii) wrapping of bacterial cells by nanosheets leading to impairment in cell movement and metabolism, and (iii) by inducing oxidative stress, either by direct generation of intracellular superoxide upon the internalization of GO or via electron transfer, resulting in oxidization of intracellular components and subsequent inactivation of the bacterial cells.[18,36,37] These mechanistic phenomena have been demonstrated to be dependent on the purity, size of nanosheets, concentration of GO and exposure time.[35,36] The small size of GO sheets in coatings seem to be more effective in deactivating the bacterial cells by generating oxidative stress due to the higher defect density,[35] whereas larger GO sheets are considered to act mainly by cell entrapment mechanisms, especially when GO is applied to bacterial cells in planktonic state.[34] The entrapment phenomenon has been speculated to be more bacteriostatic than bactericidal.[13,35] In addition to that, destructive extraction of phospholipids from bacterial cells upon interaction with graphene or GO has been demonstrated in both simulations and experiments.[38,39] Furthermore, GO was observed to have antibacterial activity against multidrug resistant pathogens.[40,41] Growth inhibition of *Klebsiella pneumoniae* by GO in a murine infection model resulted in enhanced survival of mice by preserving the viability of lung cells followed by the prevention of inflammation and tissue damage.[40] However, the observed relapse of infection depicted a failure in complete eradication of bacteria, suggesting a difference between the in vitro and in vivo antibacterial potential of GO.[40] Hence, an in-depth understanding of the molecular mechanisms by which GO demonstrates antimicrobial activity is required to design safe and effective GO-based antibacterial therapeutics.

Mass spectrometry-based proteomics analysis has been widely used to analyze bacterial response to external stimuli such as drug or nanomaterial exposure.[42–45] Quantitative proteomics analysis is often employed to analyze the expression level of proteins in a bacterial system, to gain an in-depth understanding into what pathways they regulate and to be able to construct complete signaling networks. Proteomics analysis would help to gain an insight into the dynamic behavior of proteins under the influence of various environmental conditions at any given time point. Differentially expressed proteins (relative abundance) directly reflect the changes occurring in the biological processes (sometimes in the form of feedback loops) upon drug or nanomaterial perturbations. Thus, it is crucial to understand the underlying molecular mechanisms of the bacteriostatic or bactericidal nature of a drug or nanomaterial. This information in turn could help enhance the efficiency and effective use of the said drug/nanomaterial. Thus, in this study, our aim was to explore the time-dependent antimicrobial effect of GO and perform an in-depth evaluation of the underlying molecular mechanisms, by analyzing the alteration in protein expression in *Staphylococcus aureus*.

Materials and Methods

The Preparation of Bacterial Cultures

Staphylococcus aureus subsp. *aureus* NCTC 10788 was tested in this study. The bacterial strain was purchased from the Gothenburg University Culture Collection. Tryptic soy broth (TSB)/agar was used for the cultivation and growth of the

bacteria. The inoculum was prepared by inoculating a colony of the bacterial strain in 5 mL of growth medium and incubating overnight at 37 °C.

The Examination of Graphene Oxide Nanoparticles

Highly concentrated single layered aqueous graphene oxide (GO) was purchased from Graphene Supermarket Inc., USA (SKU: UHC-GO-175ML; bottle: 6113). The concentration of the GO was 6.2 g/L with a composition of 79% carbon and 20% oxygen. The surface size of GO was in the range of 0.5 to 5 µm. The GO stock solution was diluted to 2 mg/mL and sonicated for 4 h in a sonication bath to obtain well-dispersed nanosheets in solution. The size of GO was measured by dynamic light scattering (DLS) on a Zetasizer nano (Malvern Panalytical Ltd, Malvern, UK), at room temperature, at a concentration of 10 µg/mL. Furthermore, infrared spectra of GO were recorded using an attenuated total reflectance Fourier transform infrared spectroscopy (ATR-FTIR) Alpha spectrometer (Bruker), with a diamond crystal as a refractive element, in the range 500−4000 cm^{-1} at a resolution of 4 cm^{-1}. Raman spectra was measured with a Raman microscope-WITec alpha300R equipped with a 50× objective and a 532 nm laser and 600 g/mm grating. Each spectrum was recorded in the range of 500–3000 cm^{-1}, with 10 number accumulations, and 0.5 second integration time. X-ray photoelectron spectroscopy (XPS) measurements were carried out on a PHI VersaProbe III X-ray photoelectron spectroscope using monochromatized Al Kα (1486.6 eV) X-ray source. The take-off angle was 90° relative to the surface. The data analysis was performed with CasaXPS software. Atomic force microscopy (AFM) images were carried out using INTEGRA Prima setup NT-MDT Spectrum Instruments with a resonance frequency of 150 kHz in a tapping mode. Images were recorded in 512×512 pixels, at a 0.5 Hz scan rate and then processed using the Gwyddion software.

Time Kill Assay Against *S. aureus* Using GO

Bacterial cells grown overnight were inoculated into fresh tryptic soy broth (TSB) medium (dilution factor: 200) containing sterilized deionized water ("control") or 100 µg/mL GO ("treatment"). The culture flasks were incubated at 37 °C, 300 rpm for a total of 24 h. The sample fractions (100 µL) were collected at 0 h, 4 h, 8 h and 24 h to evaluate the viability of the bacterial cells. To determine the viability, the collected culture suspension was serially diluted using isotonic saline and plated on TSB agar plates to count colonies.

Fluorescence Microscopy Analysis of the Bacteria

For live/dead staining, 500 µL of control and GO treated bacterial culture were collected at 4 h, 8 h and 24 h of growth. The collected cells were stained with LIVE/DEAD fluorescence stain kit L7012 (Invitrogen, Molecular Probes Inc., Eugene, OR, USA) containing SYTO 9 and propidium iodide. SYTO 9 crosses the bacterial membrane and binds to DNA, whereas propidium iodide can only cross the disrupted bacterial membrane. The bacterial cells were stained with a mixture of SYTO 9 and propidium iodide for 20 min and examined using a fluorescence microscope (Carl Zeiss, Jena, Germany). To examine the intracellular reactive oxygen species, 500 µL of control and GO treated bacterial culture were collected at 8 h and 24 h of growth and stained with DAPI and CellRox deep ROS sensor (Life Technologies) as reported in a previous study.[46] Briefly, the bacterial cells were stained with CellRox deep red stain for 20 min, washed with sterilized deionized water followed by counter staining with DAPI for 20 min. The stained cells were again washed with sterilized deionized water and examined under a fluorescence microscope. The acquired images were further analyzed for the quantification of different color intensities using ImageJ (National Institute of Health).

Scanning Electron Microscopy Analysis of Bacterial Cells

Scanning electron microscope was used to examine the morphology of bacterial cells after GO exposure. For SEM, 500 µL of control and GO treated bacterial culture were collected at 4 h, 8 h and 24 h of growth. The collected cells were immediately fixed overnight with 3% of glutaraldehyde. The fixed bacterial cells were dehydrated using a graded series of ethanol concentrations (40–90%) for 10 min and with 100% ethanol for 15 min. The dehydrated cells were loaded on clean glass surfaces and dried at room temperature. The dried samples were then sputter coated with gold (5 nm) prior to SEM imaging. SEM imaging was performed using JEOL JSM 6301F (Carl Zeiss AG, Jena, Germany).

Protein Extraction and Digestion from *S. aureus*

All experiments for mass spectrometry analysis were carried out in biological triplicates. For quantitative proteomics analysis, samples (1 mL) were harvested after 4 h, 8 h and 24 h of bacterial growth with and without GO treatment. The harvested samples were then centrifuged at 14,000 rpm for 5 min at 4 °C to obtain cell pellets. The acquired cell pellets were stored at −80 °C until required. Cells were lysed using a detergent-based lysis buffer containing 4% SDS in 100 mM triethylammonium bicarbonate pH 8.5 and 10 mM ethylenediaminetetraacetic acid (EDTA), along with a protease inhibitor cocktail (cOmplete™, Roche). Cell extracts were further boiled at 90 °C for 10 min, followed by sonication for 30 s on ice. Cell debris was removed by spinning down the cells at 13,400 rpm for 45 min at 4 °C. The protein lysate was purified using acetone/methanol precipitation. Dried protein pellets were resuspended in denaturation buffer containing 8 M urea in 10 mM Tris-HCl pH 8.0. 15 µg protein lysate was subjected to reduction with 1 mM dithiothreitol (DTT) and alkylation with 5.5 mM iodoacetamide (IAA) in the dark, for 1 h each at room temperature. Proteins were subsequently digested for 16 h with trypsin (1:100, w/w; Pierce™). The reaction was arrested by acidification with 10% trifluoroacetic acid and stage-tipped.[47]

NanoLC-MS/MS Analysis of Extracted Proteins

Following sample desalting using C18 stage-tips,[47] each sample was injected thrice (for label-free quantitation, LFQ) on an Easy-nLC 1200 system coupled to a Q Exactive HF-X mass spectrometer (Thermo Fisher Scientific).[48] Chromatographic separation was performed using 20 cm analytical column (75 µm ID PicoTip fused silica emitter (New Objective)) in-house packed with ReproSil-Pur C18-AQ 1.9 µm resin (Dr Maisch GmbH). The peptide mixtures were separated using an 87-minute segmented gradient from 10–90% of HPLC solvent B (80% acetonitrile in 0.1% formic acid) in HPLC solvent A (0.1% formic acid) under a flow rate of 200 nL/min. The mass spectrometer was operated in a data-dependent mode. Resolution of the Orbitrap mass analyzer was 60,000 (full MS) and 30,000 (MSMS). The 12 most intense precursor ions were sequentially fragmented in each scan cycle using higher energy collisional dissociation (HCD) fragmentation. In all measurements, dynamic exclusion was set for 30 s. The target values were 10^5 charges for MS/MS fragmentation and 3×10^6 charges for the MS scan.

Proteomic Data Analysis

Acquired MS spectra were processed using the MaxQuant software suite (version 1.6.7.0),[49] integrated with an Andromeda search engine. Database search was performed against a target-decoy database of *Staphylococcus aureus* NCTC 8325 downloaded from UniProt (taxonomy ID 93061), containing 2,889 protein entries, and additionally including 246 commonly observed laboratory contaminants. All search parameters in the MaxQuant software were maintained as default. The endoprotease was set as trypsin/P with a maximum missed cleavage of two. The fixed modification was set for carbamidomethylation (Cys). Label-free quantification was selected with a minimum ratio count of two. A false discovery rate of 1% was applied at the peptide and protein level individually. Downstream bioinformatics analysis was performed using Perseus version 1.6.15.0.[50] Data were filtered to contain entries with only quantitative information in at least 2 of the tested 6 conditions. Missing values were replaced from the normal distribution via imputation. Paired *t*-test was performed on each group (i.e., for each time point) (P-value threshold – 0.05). Only significant hits from the *t*-test were used to perform the Fisher exact test (P-value threshold – 0.05). Enrichment plots were generated using a free online platform for data analysis and visualization (bioinformatics.com.cn).

Statistical Analysis

All experiments were performed in biological triplicates and the data are presented as the mean ± standard deviation. The statistical analysis and the difference between the groups was estimated by one-way analysis of variance (ANOVA), followed by a Tukey's test to compare the multiple means. Differences between values were considered statistically significant if the *P*-value was lower than 0.05.

Results and Discussion

Characterization of Graphene Oxide (GO)

FTIR was used to determine the functional groups of the GO (Figure 1A). It exhibited the following characteristic features: the peak at 1620 cm^{-1} corresponded to the stretching vibration of C=C in the unoxidized graphitic domain, and the oxidized surface regions were evident by the stretching vibration of carboxyl C=O and bending vibration of C-OH in 1730 and 1390 cm^{-1}, respectively. The peak at 1055 cm^{-1} corresponded to the stretching vibration of C-O groups and the broad band at 3370 cm^{-1} corresponded to the OH vibration stretching.[6] GO was further analyzed by XPS to evaluate the chemical states. The survey scan spectra of GO showed the presence of carbon and oxygen (Figure 1B). High-resolution C_{1s} spectra of GO has been shown in Figure 1C. The C_{1s} spectrum of GO was characterized by contributions at 284.6, 286.8, 288.2 and 290.0 eV, arising from the C-C, C-O, C=O and O-C=O bonds, respectively.[51] Raman spectroscopy was performed to assess the level of "disorder" in the sp^2 hybrid structure of graphene family.[52] The Raman spectra of GO has been shown in Figure 1D. The G band (1585 cm^{-1}) was a result of in-plane vibrations of sp^2 bonded carbon atoms, whereas the D band (1350 cm^{-1}) was due to out-of-plane vibrations attributed to the presence of structural defects. The splitting of 2D Raman-active bands centered at 2700 cm^{-1}. The prominent D peak was from the structural imperfections created by the attachment of the hydroxyl and epoxide groups on the carbon basal plane.[53] AFM image was used to obtain the morphology and thickness of GO sheets. The AFM image (Figure 1E and F) depicted the height of GO to be 1 nm, demonstrating the single-layer thickness structure feature.[54]

Exposure Time is Key for Antimicrobial Activity of GO

The bacteriostatic and bactericidal efficiency of GO has been widely studied, and many previous studies have confirmed its broad-spectrum antimicrobial efficiency.[13–15] However, most of the studies have tested the antimicrobial properties of GO against the harvested bacterial cells in log phase and under nutrient-depleted conditions.[13,15,40,41] In practical biomedical

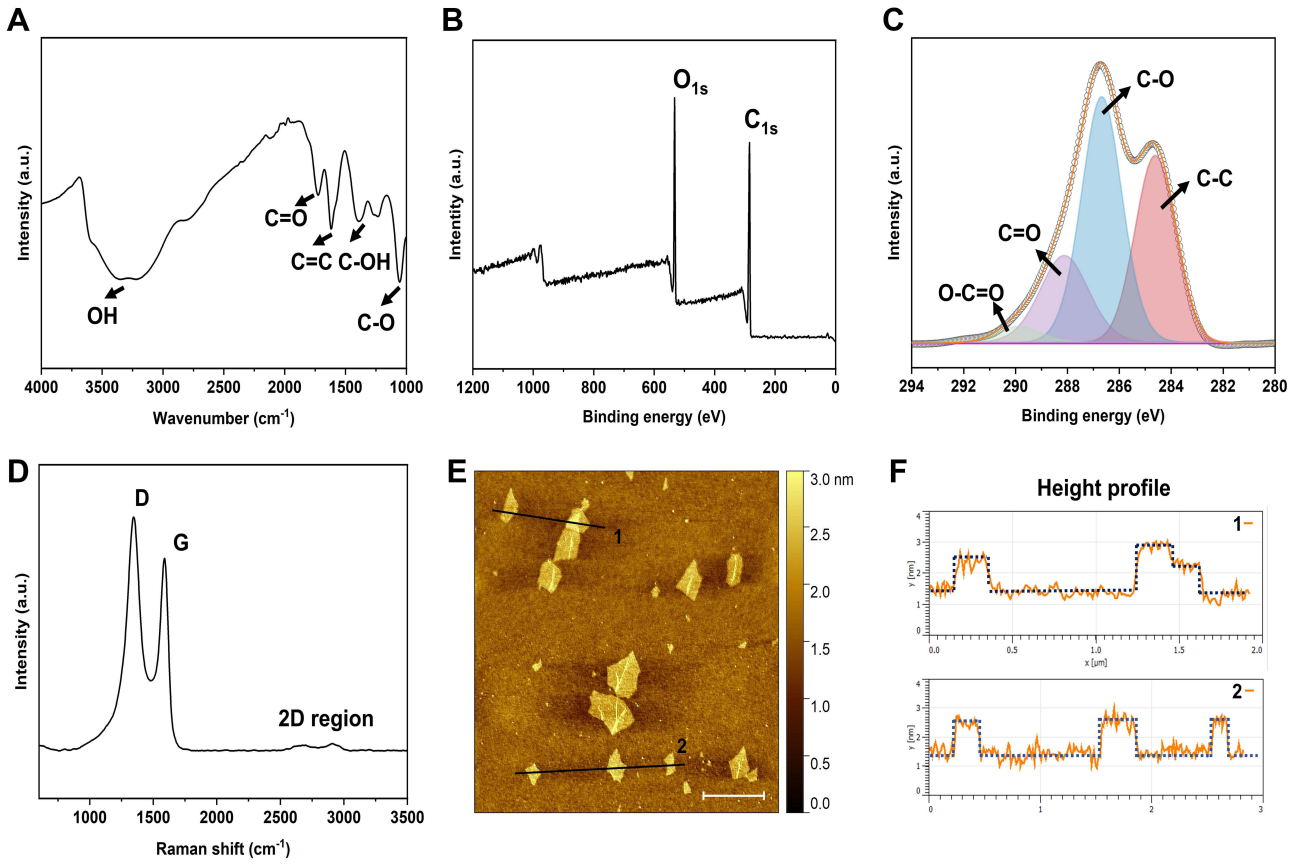

Figure 1 Characterization of GO. (**A**) IR spectra of GO sheet; (**B**) XPS of survey spectra of GO; (**C**) C1s core level spectrum of GO; (**D**) Raman spectra of the GO; (**E** and **F**) AFM analysis of GO.

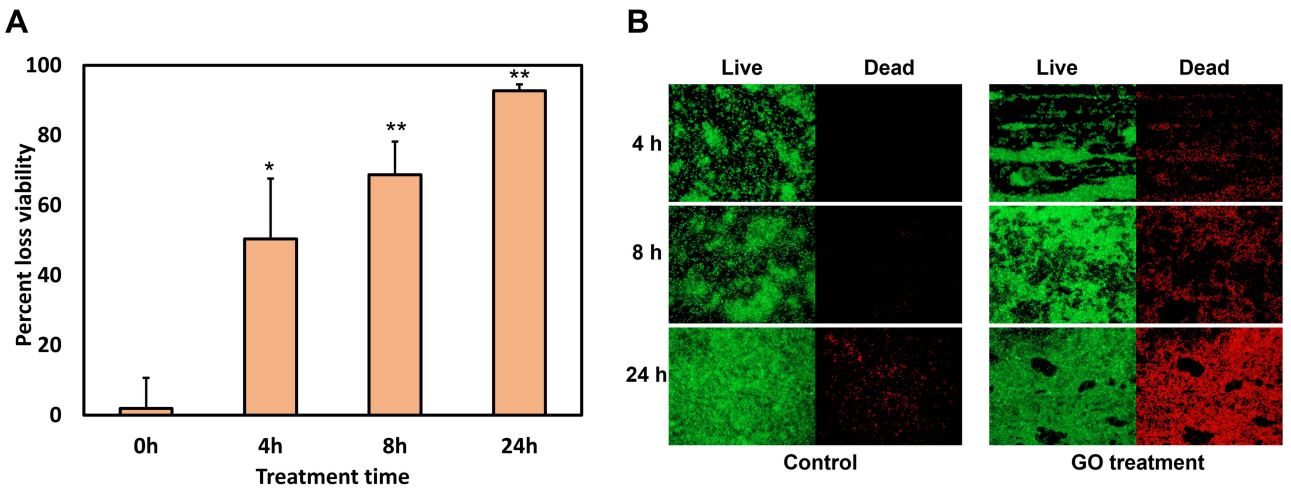

Figure 2 Time-dependent bactericidal activity of GO. (**A**) Loss of viability of *S. aureus* upon GO treatment for 4 h, 8 h and 24 h in comparison to control sample. (**B**) Representative fluorescence microscopy images of control and GO-treated *S. aureus* cells for 4 h, 8 h and 24 h. Green color represents live bacterial cells and red color represents dead bacterial cells. Data represented as mean ± standard deviation from three independent biological replicates. *P <0.01, **P <0.0001.

applications, bacterial cells are likely to be exposed to a variety of nutrients, hence in this study we examined the antibacterial efficiency of GO and its mode of action in the presence of a rich medium. The bacterial cells were exposed to GO, and samples were collected at 4 h, 8 h and 24 h of culture time to test the viability of the bacteria, morphological alteration, and changes in the protein expression of the bacterial cells induced by GO treatment. Since the smaller size of GO has been demonstrated to have higher antimicrobial efficacy as previously mentioned,[35,36] an average size of 90 ± 2 nm GO was selected for this study. The size of GO was optimized by sonication of commercial GO for 2 h. Control and GO-exposed bacterial cultures were collected at 4 h, 8 h, and 24 h of growth and bacterial viability was analyzed and represented as CFUs. In accordance with previous studies, GO was observed to significantly reduce bacterial viability. As shown in Figure 2A, GO treatment reduced 50 ± 17% of the viability of bacterial cells after 4 h of exposure time, 69 ± 9% after 8 h, and 93 ± 2% after 24 h of treatment, suggesting that exposure time is a key factor in achieving a strong antimicrobial effect. This observation also eliminates any speculation that a rich medium may alter the bioactivity of GO and reduce its antimicrobial property,[55] thus highlighting the fact that GO is equally effective in deactivating bacterial cells that are enriched with nutrients.

The wrapping and trapping of bacterial cells in planktonic state by GO was demonstrated previously as a leading mode of action for antimicrobial activity.[13,24,34] Furthermore, the role of such wrapping by GO was speculated to mainly inhibit the bacterial growth by preventing proliferation rather than killing the bacterial cells.[56] Hence to examine the bactericidal effect of GO against the planktonic bacterial cells, the treated and non-treated cells were examined by fluorescence microscopy after staining them with a Live/Dead viability stain. The staining kit contains two different fluorescent dyes - SYTO 9 and propidium iodide. Both are nucleic acid stains, but SYTO 9 is cell membrane permeable and can thus enter live cells and stain them green. Propidium iodide on the other hand being impermeable to cell membranes can only stain cells with disrupted membranes red. This is a well-established method to visualize the live and dead bacterial cells and can help to distinguish the bacteriostatic and bactericidal effect of antimicrobial drugs or nanomaterials. Figure 2B illustrates the density of viable and non-viable bacterial cells with and without GO treatment. The density of non-viable cells (red color) was observed to increase with increasing GO exposure time (Figure 2B). This observation strongly suggests that GO treatment against planktonic bacteria not only has a bacteriostatic effect but also deactivates the cells by disrupting the cell membrane.

Combination of Wrapping, Contact Killing, and Generation of ROS Attributes to the Antimicrobial Potential of GO

The size and concentration dependent antimicrobial activity of GO has been shown previously.[35,36] Studies have also demonstrated wrapping of bacterial cells by GO as a dominant factor in terms of antimicrobial activity against bacterial cells in planktonic stage.[13,35] Physical damage of bacterial cells by sharp edges of vertical GO coatings has also been

reported.[6,17] To understand the exact mechanism of action of GO against planktonic bacteria, control and GO-treated bacteria were harvested and examined using SEM and CellRox staining to determine the morphological alteration and intracellular ROS respectively.

As shown in Figure 3A, significant wrapping of bacterial cells was observed even at 4 h of GO treatment. The intensity of wrapping/trapping of bacterial cells was dependent on the duration of treatment time (Figure S1). Although wrapping of cells was evident after 4 h of GO exposure, very few bacterial cells were observed to have severe

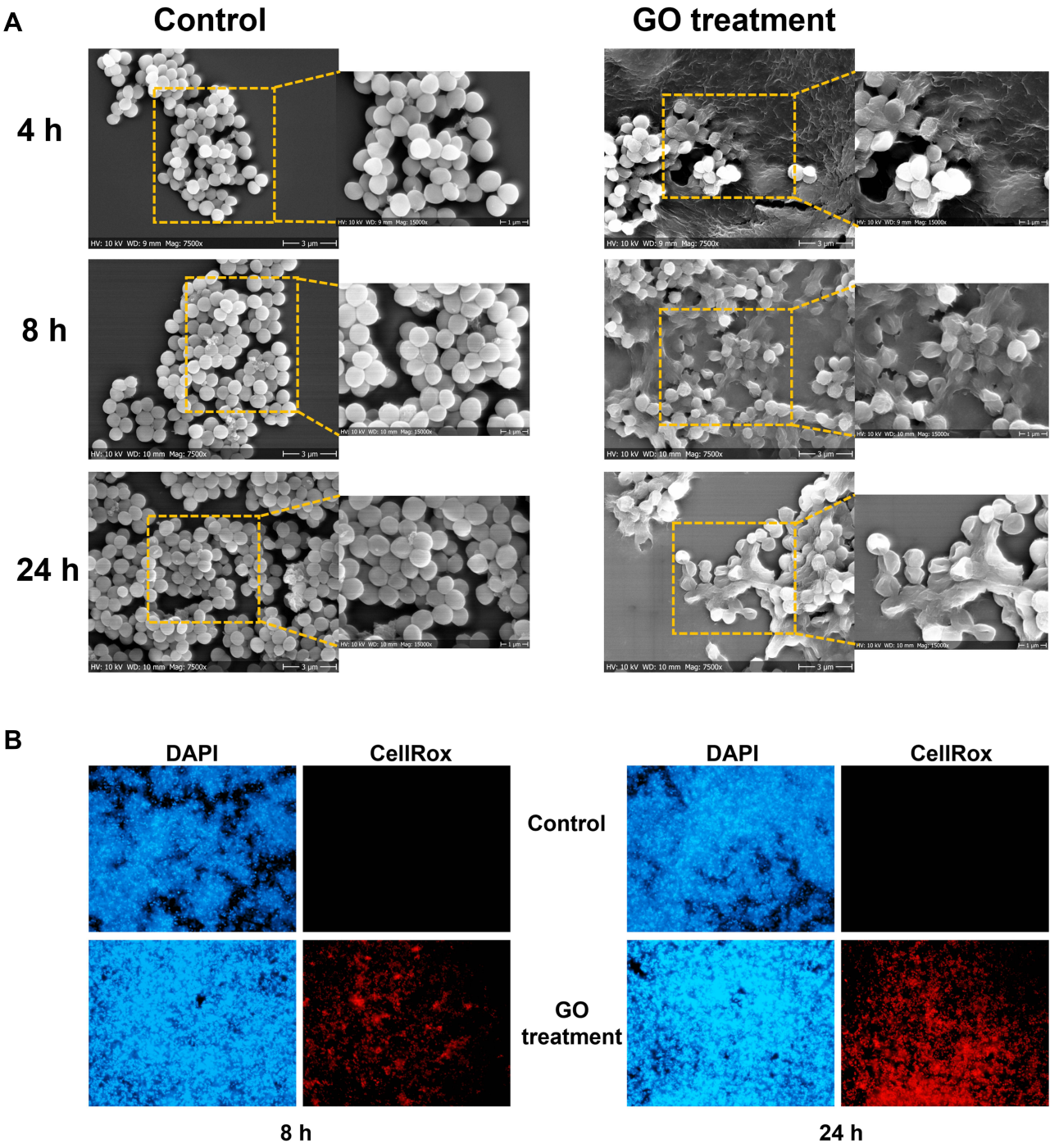

Figure 3 Efficiency of GO to deactivate *S. aureus* cells and generation of intracellular reactive oxygen species is dependent on exposure time. (**A**) Representative scanning electron microscopy images of control and GO-treated *S. aureus* cells for 4 h, 8 h and 24 h respectively. (**B**) Representative fluorescence microscopy images depicting generation of intracellular ROS in *S. aureus* cells after 8 h and 24 h of GO treatment respectively. Blue color represents bacterial cells and red color represents the ROS.

morphological disruption. In addition to wrapping, the morphological damage in terms of membrane perturbation (hole-like structures) and collapse of cell membranes leading to complete disintegration of cells was observed after 8 h of GO exposure. The increase in severity of membrane disruption and density of damaged cells was observed after 8 h and 24 h of exposure time suggesting that longer exposure time might be needed to achieve a contact-killing effect. Furthermore, generation of intracellular ROS has been suggested previously as another mode of action by which GO deactivated the bacterial cells.[14,24,34,35] However, most of those assays were done in vitro by evaluating its glutathione reduction ability. The actual intracellular ROS generation by GO in bacterial cells was rarely investigated. In order to examine the generation of intracellular ROS, bacterial cells exposed to GO for different times were collected, stained with deep red ROS fluorescence stain and examined using a fluorescence microscope. As shown in Figure 3B, GO exposure resulted in generation of intracellular ROS. A significant amount of ROS in bacterial cells was detected after the 8 h of GO treatment. Furthermore, an increase in amount of intracellular ROS was observed in the bacterial cells treated with GO for 24 h, suggesting that exposure time is key to achieve ROS mediated bactericidal activity. As expected, ROS was not detected in control cells that were not exposed to GO. The results obtained here confirm that intracellular ROS generation on GO exposure occurs in vivo as well, which previously was demonstrated in vitro by glutathione reduction. However, the amount of intracellular ROS after 24 h of GO treatment was less pronounced than the extent of dead cells after live/dead staining (Figure 4). This observation indicates that the bactericidal activity of GO depends not only on ROS generation, but rather is a combinatorial effect including other killing factors as well, namely wrapping/trapping and insertion (Figures 2 and 3). For instance, our SEM and ROS staining observation suggests that the antimicrobial activity of GO against planktonic bacterial cells begins with wrapping and trapping and is later followed by insertion and ROS generation with increasing treatment time.

Label-Free Quantitative (LFQ) Proteomic Analysis of *S. aureus*

Label-free quantitative proteomics has been widely employed to determine the relative abundance of proteins amongst biological samples subjected to diverse treatment conditions, without having the need to perform additional expensive chemical labeling workflows. In the current study, in order to examine the alteration in protein expression induced by GO treatment, label-free quantitative proteomics analysis was employed. 1,524 proteins were overall identified of which 1,078 were quantified in at least 50% of the tested conditions (Supplementary Table 1). Experiments were conducted in biological triplicates as well as technical triplicates. The three biological replicates showed a high degree of correlation (Pearson correlation coefficient ≥ 0.9) (Figure S2). A histogram plotted of all the replicates, under all assessed conditions, depicted normal distribution of the data (Figure S3). Volcano plots depicting differentially regulated proteins in both directions ($P < 0.05$) across all time points, indicated a dynamic fluctuation of protein expression at the molecular level

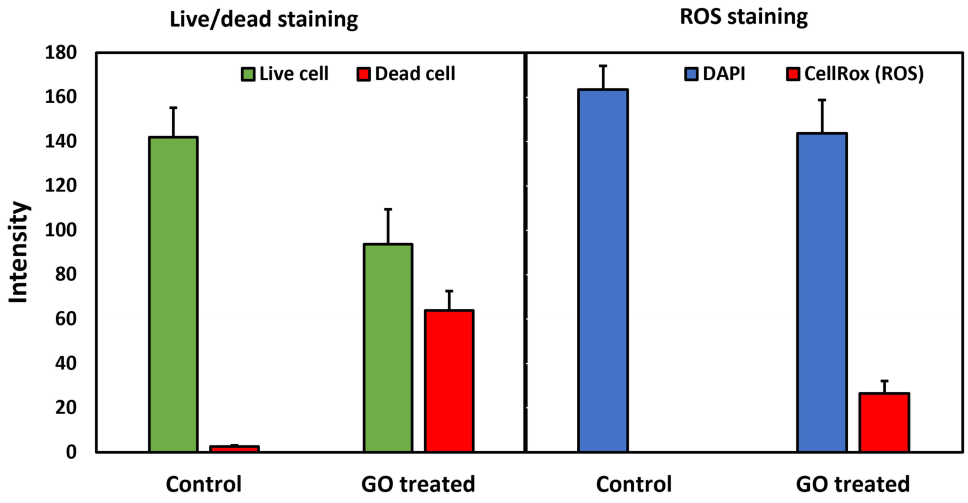

Figure 4 Quantification of fluorescence color intensity of images acquired from live/dead viability staining and ROS staining. Fluorescence images acquired after 24 h of GO treatment were used for intensity quantification. Data represent mean ± standard deviation from three independent biological replicates.

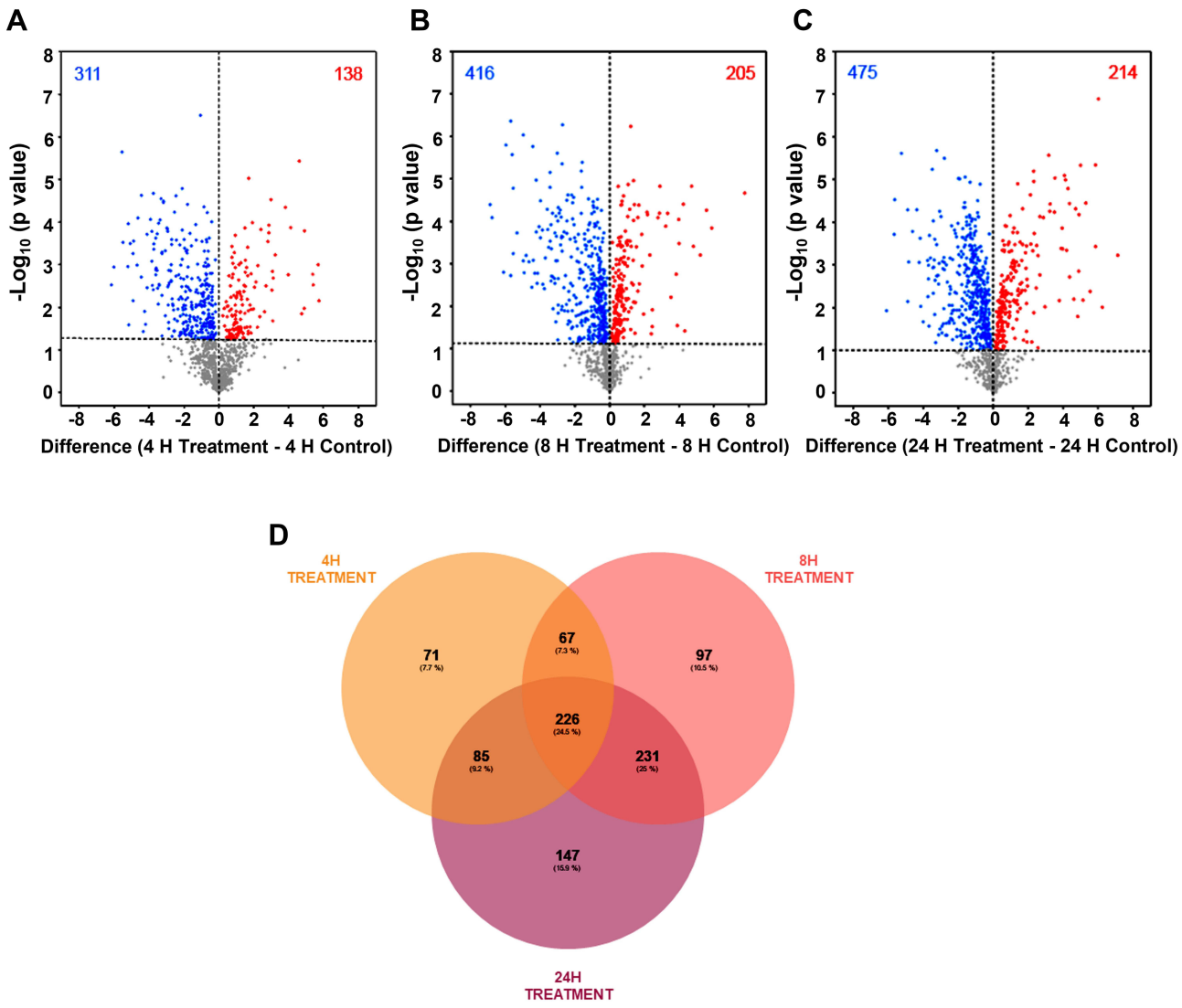

Figure 5 Volcano plots depicting differentially expressed protein levels between GO treatment and control conditions at (**A**) 4 h, (**B**) 8 h and (**C**) 24 h. The horizontal black dotted line represents significance threshold at FDR 0.05. Significantly up- and down-regulated proteins on GO treatment are denoted in red and blue colours respectively. (**D**) Venn diagram depicting intersection of data - overlap between significantly regulated proteins (P <0.05) after 4 h, 8 h and 24 h of GO treatment.

(Figure 5A–C). As the time of GO treatment increased, expression of a greater number of proteins was observed to be significantly affected (Figure 5D). Gene ontology enrichment plots of the significantly regulated proteins indicated an over-representation of terms related to oxidative stress response, general stress response and ion transport (Figure 6A–C). Additionally, a large number of cell-membrane associated proteins were also seen to be differentially regulated (Figure 6A–C); 226 proteins were identified to be significantly regulated across all three tested GO treatment time points (4 h, 8 h and 24 h).

Proteins downregulated upon GO treatment included those associated with cytolysis, peptidoglycan catabolic process, cell wall biogenesis and proteins associated with oxidative stress. Large number of proteins that are associated with biosynthesis of cell wall and peptidoglycan were also found to be downregulated. Notably, LtaS, MGT, MsrR, ebh, MurB, MurC, TagGH and TarL were found to be significantly downregulated upon GO treatment. The LtaS protein which was downregulated by 3.7-fold after 4 h of GO treatment, is known to interact with proteins (associated with early and late cell division) and enzymes that play an intrinsic role in peptidoglycan synthesis.[57] Another downregulated protein MGT is actively expressed in *S. aureus* and considered as an important member of membrane-associated protein. This protein has been suggested to play a significant role in bacterial cell wall biosynthesis.[58] The protein MsrR was also

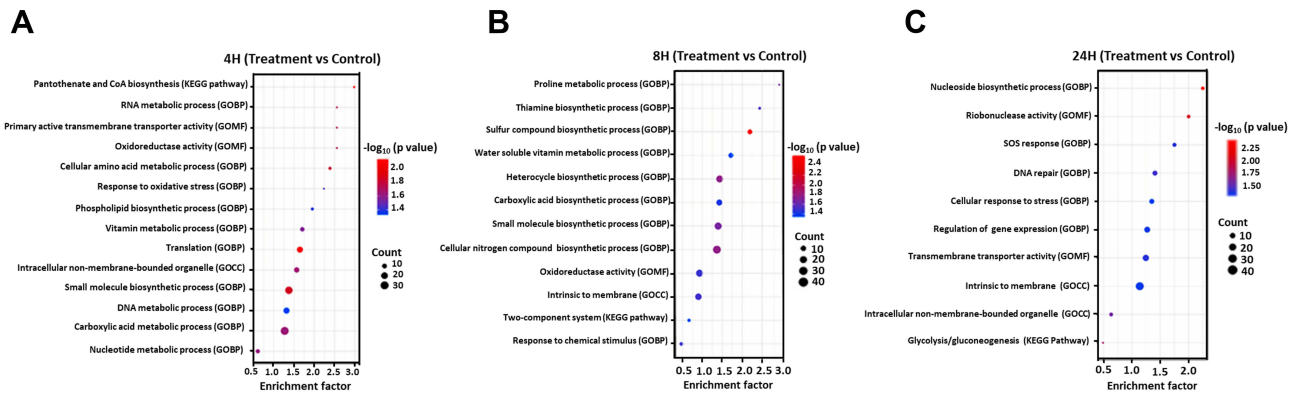

Figure 6 Enrichment plots depicting gene ontology terms/KEGG pathways that are affected on GO treatment after (**A**) 4 h, (**B**) 8 h and (**C**) 24 h respectively. The color of the dots indicates the P-value of enrichment significance and the size of the dots represents the number of proteins falling under the corresponding category. Only the most significant hits (P <0.05) are represented in the plot.

found to be downregulated by 1.5-fold in *S. aureus* treated with GO for 24 h. MsrR belongs to the LytR-CpsA-Psr family of cell envelope-associated proteins and has been suggested to play a significant role in cell envelope maintenance, cell separation and pathogenicity of *S. aureus*.[59] Protein Ebh was downregulated by 1.8-fold in the cells treated with GO for 24 h. The mutation in *ebh* has been previously demonstrated to increase the cell growth, but observed to affect the cross wall, membrane enclosed peptidoglycan synthesis and assembly compartment.[60] MurB, a protein that plays a critical role to reduce UDP-GlcNAcEP to UDP-*N*-acetylmuramic acid in the process of peptidoglycan biosynthesis,[61] was also downregulated by 1.6-fold after 24 h of GO treatment. On the other hand, MurC, that also plays a major role in peptidoglycan and cell wall biosynthesis,[62] was found to be downregulated by 1-fold and 1.7-fold respectively after 8 h and 24 h of GO treatment. Interestingly, another protein RpiA was downregulated by 2.9-fold and 3.4-fold respectively in *S. aureus* cells treated with GO for 8 h and 24 h. Previously, *rpiA* mutants were observed with alteration in gene expression which are associated with peptidoglycan synthesis such as upregulation of *mecA* and *sgtB*, and down-regulation of *murBJY, femABX, pbp4, ftsW* and *rodA*.[63] Another protein TagH was also found to be downregulated by 1.1-fold in *S. aureus* upon 24 h of GO treatment. This protein is a membrane-bound component of the teichoic acid translocation system and is involved in teichoic acid synthesis. The depletion in this protein was previously found to thicken the cell wall due to autolysin sequestration.[64] In addition to this TarL protein, which is believed to be involved in synthesis of the ribitol phosphate polymer of cell wall teichoic acid by using the activated precursor, CDP-ribitol,[65] was found to be drastically downregulated upon GO treatment. TarL was downregulated by 2.1-fold, 3.5-fold and 3.6-fold in *S. aureus* after 4 h, 8 h and 24 h of GO treatment respectively.

The second largest group of proteins that were affected by GO treatment were associated with oxidative stress (Figure 7A–C). Notably proteins AldA, ClpC and Msr that are linked to oxidative stress were found to be highly downregulated. The protein AldA was downregulated (2.3-fold) in *S. aureus* only after 24 h of GO treatment. AldA was previously found to be irreversibly inhibited under H_2O_2 treatment via overoxidation of Cys279 demonstrating its sensitivity to oxidative stress. In addition to that, AldA was also found to be sensitive to NaOCl stress.[66] On other hand, clpC operon in *S. aureus* comprises of four different genes: *ctsR, mcsA, mcsB* and *clpC*. The disruption in clpC was demonstrated to result in hypersensitivity to heavy metal stress, temperature stress, osmotic pressure stress, oxidative stress, and alteration in biofilm formation.[67] Msr protein in *S. aureus* was also found to be highly downregulated upon GO treatment. The strong activity of Msr has also been demonstrated to enhance the sensitivity of various organisms to oxidative stress.[59] In addition to that quinol oxidase, and quinone oxidoreductase were also significantly downregulated after 8 h and 24 h of GO treatment. These proteins are mainly involved in cellular response to oxidative stress for cell survival.[68–70] This phenomenon suggests that GO-associated oxidative stress significantly starts after a certain period of GO exposure to bacterial cells. In addition to that, outer membrane proteins were also found to be drastically affected, wherein the majority of such proteins were found to be downregulated in all the tested treatment times, suggesting that GO effectively interacts with membrane proteins (Figure 7A–C). This could possibly be due to the wrapping/trapping

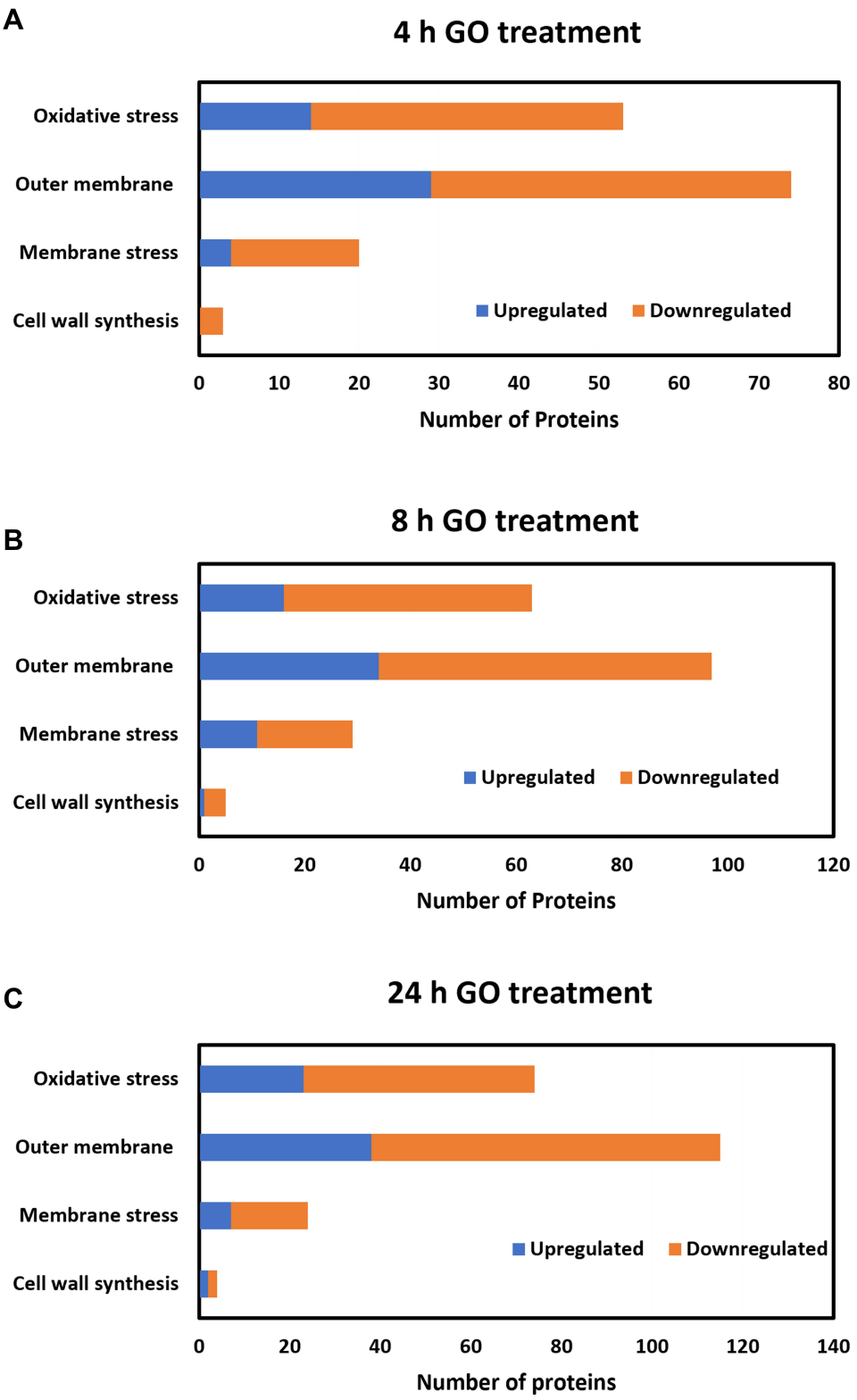

Figure 7 Number of differentially regulated proteins that are associated with oxidative stress, outer membrane, membrane stress and cell wall synthesis on graphene treatment for (**A**) 4 h, (**B**) 8 h and (**C**) 24 h.

and insertion effect of GO sheets, that increase in efficiency with increasing treatment time (Figure 3A). Moreover, GO treatment was found to downregulate several proteins in *S. aureus* that are associated with general bacterial physiology such as growth, cell division, virulence, and survival. The protein DivIB which is required for correct assembly of the divisome at midcell during division and to prevent the hydrolytic growth of the cells in the case of incomplete septum[71] was downregulated after 8 h (1-fold) and 24 h (1.2-fold) of GO treatment. Another protein FMT was found to be drastically downregulated in *S. aureus* upon GO treatment. FMT was found to be downregulated by 4.1-fold and 4.3-fold respectively after 8 h and 24 h of GO treatment. The depletion of this protein has been suggested to reduce the cell growth rate and virulence properties.[72] The protein HslO which is known as a death resistance protein and acts as a protective factor for cells during the stress condition,[73] was found to be greatly downregulated with the GO treatment. HslO was found to be downregulated by 3-fold, 5.5-fold and 4.6-fold respectively after 4 h, 8 h and 24 h of GO treatment. Another protein, IcaR, was also found to be downregulated at all time points of GO exposure. This protein encodes a repressor of *icaADBC* transcription in *S. aureus* and is known to significantly impact the cell adhesion and biofilm formation.[74] IcaR was found to be downregulated by 3.4-fold, 3.1-fold and 4.8-fold respectively after 4 h, 8 h and 24 h of GO treatment.

By contrast, some proteins associated with oxidative stress, general stress, cell growth, virulence factor and biofilm formation were found to be significantly upregulated in *S. aureus* upon GO treatment. Notably AhpC was drastically upregulated in *S. aureus* exposed to GO. AhpC was upregulated by 1.5-fold, 2.4-fold and 2.8-fold respectively after 4 h, 8 h and 24 h of GO treatment. The resistance to oxidative stress by *S. aureus* is associated with metal ion homeostasis through various regulators. For instance, PerR was found to control the expression of regulon of genes which encode antioxidants,[75] where ahpC is one of the major PerR regulon.[75] The mutation of *ahpC* has previously demonstrated to increase H_2O_2 resistance due to greater *katA* expression via relief of PerR repression.[75] Several key proteins associated with cell wall and general stress namely PrsA, VraR, FtsH, were also significantly upregulated in GO-treated *S. aureus*. PrsA was upregulated by 4.3-fold only after 24 h of GO treatment. PrsA is a membrane-anchored lipoprotein that facilitates the folding of exported proteins in the microenvironment of the cytoplasmic membrane and cell wall interface affecting the surface properties and virulence of *S. aureus*.[76] Thus, PrsA is considered as a key element of the VraRS-mediated cell wall stress response. VraR, which was upregulated in 8 h (0.8-fold) and 24 h (2.1-fold) GO-treated cells, is an essential protein for the phosphorylation-induced activation of VraR and has been shown to disrupt the cell wall stress leading to re-sensitization of cells to antibiotics.[77] FtsH is a membrane-bound metalloprotease which plays a major role in virulence properties and stress tolerance. The knockout mutation in *ftsH* has been demonstrated to increase thickness of cell walls.[78] FtsH was drastically upregulated by 3.8-fold and 5.1-fold respectively after 8 h and 24 h of treatment. In addition to that, the proteins GuaA, Spx, ThyA and YbeY were found to be significantly upregulated. These proteins are mainly associated with cell growth, virulence factors, biofilm formation and response to general stress. Moreover, enzymatic proteins such as hydrolases, proteases, peptidases, and proteins associated with cell wall biogenesis were also upregulated. Some proteins were found to be distinctly altered at specific time points of GO treatment. For instance, at 24 h of GO treatment, 13 distinct proteins were differentially regulated. Endonucleases responsible for DNA repair, exotoxins linked to pathogenesis, outer membrane proteins and lipoteichoic acid synthetases associated with biogenesis and organization of cell wall were significantly upregulated in *S. aureus* after 24 h of GO treatment, suggesting an increase in cell membrane as well as ROS associated stress with an increase in treatment time. This observation is consistent with the results obtained from SEM and ROS staining. In general, most of the upregulated proteins are mainly involved in cell adhesion, pathogenesis, cell wall biogenesis, cytolysis, and lipid catabolic process. All the fold change values mentioned above are in log2 scale.

Conclusion

In conclusion, this study reveals a time-dependent antimicrobial activity of GO against *S. aureus*. The mode of antimicrobial action observed is a combination of wrapping/trapping, insertion, and generation of intracellular ROS. While the wrapping/trapping effect was observed to be a predominant antimicrobial behavior of GO against planktonic state bacteria, oxidative stress, and membrane stress associated with cell damage and leakage of intracellular content was found as an additional mechanism. Overall, the antimicrobial action was found to begin with wrapping/trapping and the

antimicrobial efficiency was accelerated subsequently later by GO insertion and generation of significant amounts of ROS to deactivate the bacterial cells. These phenomena are confirmed by viability assessment, live/dead staining, examination of intracellular ROS and quantification of protein expression of *S. aureus* after GO treatment at different time points. Proteomics data reveal the alteration in a large number of proteins that are associated with biosynthesis of cell wall and peptidoglycan, oxidative stress, general stress response, virulence factor, cell survival and biofilm formation in GO-treated *S. aureus*. The demonstrated results in this study could provide a deeper insight into the molecular mechanism by which GO exhibits bacteriostatic and bactericidal activity, which further can be used as a guide to advance the use of GO as an antimicrobial agent in various applications and to enhance its bacteriostatic and bactericidal effect.

Acknowledgments

This work was funded by grants from the Vetenskapsrådet to SP and NordForsk and the Independent Research Fund Denmark - FNU to IM. We would like to thank Dr. Jian Zhang for his contribution in characterization of graphene oxide. This work was performed in part at Myfab Chalmers. We would like to thank the Proteome Center Tübingen, Interfakultäres Institut für Zellbiologie, Universität Tübingen, Germany, for the mass spectrometry analysis. The mass spectrometry proteomics data have been deposited to the ProteomeXchange Consortium via the PRIDE[79] partner repository with the dataset identifier PXD036796.

Disclosure

The authors report no conflicts of interest in this work.

References

1. Panda S, Rout TK, Prusty AD, Ajayan PM, Nayak S. Electron transfer directed antibacterial properties of graphene oxide on metals. *Adv Mater*. 2018;30:1702149.
2. Qiu J, Wang D, Geng H, et al. How oxygen-containing groups on graphene influence the antibacterial behaviors. *Adv Mater Interface*. 2017;4:1700228. doi:10.1002/admi.201700228
3. Reina G, González-Domínguez JM, Criado A, et al. Promises, facts and challenges for graphene in biomedical applications. *Chem Soc Rev*. 2017;46:4400–4416. doi:10.1039/C7CS00363C
4. Zou X, Zhang L, Wang Z, Luo Y. Mechanisms of the antimicrobial activities of graphene materials. *J Am Chem Soc*. 2016;138:2064–2077. doi:10.1021/jacs.5b11411
5. Weaver CL, LaRosa JM, Luo X, Cui XT. Electrically controlled drug delivery from graphene oxide nanocomposite films. *ACS Nano*. 2014;8:1834–1843. doi:10.1021/nn406223e
6. Zhao C, Pandit S, Fu Y, et al. Graphene oxide based coatings on nitinol for biomedical implant applications: effectively promote mammalian cell growth but kill bacteria. *RSC Adv*. 2016;6:38124–38134. doi:10.1039/C6RA06026A
7. Cheng J, Liu J, Wu B, et al. Graphene and its derivatives for bone tissue engineering: in vitro and In vivo evaluation of graphene-based scaffolds, membranes and coatings. *Front Bioeng Biotechnol*. 2021;9:734688. doi:10.3389/fbioe.2021.734688
8. Abdelhamid HN, Wu HF. Multifunctional graphene magnetic nanosheet decorated with chitosan for highly sensitive detection of pathogenic bacteria. *J Mater Chem B*. 2013;1:3950–3961.
9. Khan MS, Abdelhamid HN, Wu HF. Near infrared (NIR) laser mediated surface activation of graphene oxide nanoflakes for efficient antibacterial, antifungal and wound healing treatment. *Colloids Surf B Biointerfaces*. 2015;127:281–291.
10. Chen J, Peng H, Wang X, et al. Graphene oxide exhibits broad-spectrum antimicrobial activity against bacterial phytopathogens and fungal conidia by intertwining and membrane perturbation. *Nanoscale*. 2014;6:1879–1889. doi:10.1039/C3NR04941H
11. He JL, Zhu XD, Qi ZN, et al. Killing dental pathogens using antibacterial graphene oxide. *ACS Appl Mater Interface*. 2015;7:5605–5611. doi:10.1021/acsami.5b01069
12. Pulingam T, Thong KL, Ali ME, et al. Graphene oxide exhibits differential mechanistic action towards Gram-positive and Gram-negative bacteria. *Colloids Surf B Biointerfaces*. 2019;181:6–15. doi:10.1016/j.colsurfb.2019.05.023
13. Akhavan O, Ghaderi E, Esfandiar A. Wrapping bacteria by graphene nanosheets for isolation from environment, reactivation by sonication, and inactivation by near- infrared irradiation. *J Phys Chem B*. 2011;115:6279–6288. doi:10.1021/jp200686k
14. Gurunathan S, Han JW, Dayem AA, Eppakayala V, Kim JH. Oxidative stress-mediated antibacterial activity of graphene oxide and reduced graphene oxide in *Pseudomonas aeruginosa*. *Int J Nanomedicine*. 2012;7:5901–5914. doi:10.2147/IJN.S37397
15. Palmieri V, Bugli F, Lauriola MC, et al. Bacteria meet graphene: modulation of graphene oxide nanosheet interaction with human pathogens for effective antimicrobial therapy. *ACS Biomater Sci Eng*. 2017;3:619–627. doi:10.1021/acsbiomaterials.6b00812
16. Pandit S, Gaska K, Kádár R, Mijakovic I. Graphene-based antimicrobial biomedical surfaces. *ChemPhysChem*. 2020;22:250–263. doi:10.1002/cphc.202000769
17. Lu X, Feng X, Werber JR, et al. Enhanced antibacterial activity through the controlled alignment of graphene oxide nanosheets. *Proc Natl Acad Sci U S A*. 2017;114:E9793–E9801. doi:10.1073/pnas.1710996114
18. Chen Y, Pandit S, Rahimi S, Mijakovic I. Interactions between graphene-based materials and biological surfaces: a review of underlying molecular mechanisms. *Adv Mater Interface*. 2021;8:2101132. doi:10.1002/admi.202101132

19. Aydoğan C, Aslan H, Günyel Z, et al. Graphene oxide-octadecylsilane incorporated monolithic nano-columns with 50 µm id and 100 µm id for small molecule and protein separation by nano-liquid chromatography. *Electrophoresis*. 2021;42:2637–2646. doi:10.1002/elps.202100050
20. Günyel Z, Aslan H, Demir N, Aydoğan C. Nano-liquid chromatography with a new nano-structured monolithic nanocolumn for proteomics analysis. *J Sep Sci*. 2021;44:3996–4004. doi:10.1002/jssc.202100454
21. Pandit S, Cao ZJ, Mokkapati VRSS, et al. Vertically aligned graphene coating is bactericidal and prevents the formation of bacterial biofilms. *Adv Mater Interface*. 2018;5:1701331. doi:10.1002/admi.201701331
22. Pandit S, Gaska K, Mokkapati VR, et al. Precontrolled alignment of graphite nanoplatelets in polymeric composites prevents bacterial attachment. *Small*. 2020;16:1904756. doi:10.1002/smll.201904756
23. Hu W, Peng C, Luo W, et al. Graphene-based antibacterial paper. *ACS Nano*. 2010;4:4317–4323. doi:10.1021/nn101097v
24. Liu S, Zeng TH, Hofmann M, et al. Antibacterial activity of graphite, graphite oxide, graphene oxide, and reduced graphene oxide: membrane and oxidative stress. *ACS nano*. 2011;5:6971–6980. doi:10.1021/nn202451x
25. Zou F, Zhou H, Jeong DY, et al. Wrinkled surface-mediated antibacterial activity of graphene oxide nanosheets. *ACS Appl Mater Interface*. 2017;9:1343–1351. doi:10.1021/acsami.6b15085
26. Krishnamoorthy K, Veerapandian M, Zhang L, Yun K, Kim SJ. Antibacterial efficiency of graphene nanosheets against pathogenic bacteria via lipid peroxidation. *J Phys Chem C*. 2012;116:17280–17287. doi:10.1021/jp3047054
27. Lammel T, Boisseaux P, Fernández-Cruz ML, Navas JM. Internalization and cytotoxicity of graphene oxide and carboxyl graphene nanoplatelets in the human hepatocellular carcinoma cell line Hep G2. *Part Fibre Toxicol*. 2013;10:27. doi:10.1186/1743-8977-10-27
28. Zhang J, Cao HY, Wang JQ, Wu GD, Wang L. Graphene oxide and reduced graphene oxide exhibit cardiotoxicity through the regulation of lipid peroxidation, oxidative stress, and mitochondrial dysfunction. *Front Cell Dev Biol*. 2021;9:616888. doi:10.3389/fcell.2021.616888
29. Choudhary P, Parandhaman T, Ramalingam B, et al. Fabrication of nontoxic reduced graphene oxide protein nanoframework as sustained antimicrobial coating for biomedical application. *ACS Appl Mater Interface*. 2017;9:38255–38269. doi:10.1021/acsami.7b11203
30. Mohammed H, Kumar A, Bekyarova E, et al. Antimicrobial mechanisms and effectiveness of graphene and graphene-functionalized biomaterials. A scope review. *Front Bioeng Biotechnol*. 2020;8:465.
31. Mandal P, Ghosh SK, Grewal HS. Graphene oxide coated aluminium as an efficient antibacterial surface. *Environ Technol Innov*. 2022;28:102591.
32. Soenen SJ, Parak WJ, Rejman J, Manshian B. (Intra)cellular stability of inorganic nanoparticles: effects on cytotoxicity, particle functionality, and biomedical applications. *Chem Rev*. 2015;115:2109–2135. doi:10.1021/cr400714j
33. Wang D, Lin Z, Wang T, et al. Where does the toxicity of metal oxide nanoparticles come from: the nanoparticles, the ions, or a combination of both? *J Hazard Mater*. 2016;308:328–334. doi:10.1016/j.jhazmat.2016.01.066
34. Liu S, Hu M, Zeng TH, et al. Lateral dimension-dependent antibacterial activity of graphene oxide sheets. *Langmuir*. 2012;28:12364–12372. doi:10.1021/la3023908
35. Perreault F, de Faria AF, Nejati S, Elimelech M. Antimicrobial properties of graphene oxide nanosheets: why size matters. *ACS Nano*. 2015;9:7226–7236. doi:10.1021/acsnano.5b02067
36. Anand A, Unnikrishnan B, Wei SC, et al. Graphene oxide and carbon dots as broad-spectrum antimicrobial agents - a minireview. *Nanoscale Horiz*. 2019;4:117–137. doi:10.1039/C8NH00174J
37. Radhi A, Mohamad D, Abdul Rahman FS, Abdullah AM, Hasan H. Mechanism and factors influence of graphene-based nanomaterials antimicrobial activities and application in dentistry. *J Mater Res Technol*. 2021;11:1290–1307. doi:10.1016/j.jmrt.2021.01.093
38. Tu Y, Lv M, Xiu P, et al. Destructive extraction of phospholipids from *Escherichia coli* membranes by graphene nanosheets. *Nat Nanotechnol*. 2013;8:594–601. doi:10.1038/nnano.2013.125
39. Wu L, Zeng L, Jiang X. Revealing the nature of interaction between graphene oxide and lipid membrane by surface-enhanced infrared absorption spectroscopy. *J Am Chem Soc*. 2015;137:10052–10055. doi:10.1021/jacs.5b03803
40. Wu X, Tan S, Xing Y, et al. Graphene oxide as an efficient antimicrobial nanomaterial for eradicating multi-drug resistant bacteria in vitro and in vivo. *Colloids Surf B Biointerfaces*. 2017;157:1–9. doi:10.1016/j.colsurfb.2017.05.024
41. Aunkor MTH, Raihan T, Prodhan SH, et al. Antibacterial activity of graphene oxide nanosheet against multidrug resistant superbugs isolated from infected patients. *R Soc Open Sci*. 2020;7:200640. doi:10.1098/rsos.200640
42. Pandit S, Ravikumar V, Abdel-Haleem AM, et al. Low concentrations of vitamin C reduce the synthesis of extracellular polymers and destabilize bacterial biofilms. *Front Microbiol*. 2017;8:2599. doi:10.3389/fmicb.2017.02599
43. Yan X, He B, Liu L, et al. Antibacterial mechanism of silver nanoparticles in *Pseudomonas aeruginosa*: proteomics approach. *Metallomics*. 2018;10:557–564. doi:10.1039/C7MT00328E
44. Zhang Y, Pan X, Liao S, et al. Quantitative proteomics reveals the mechanism of silver nanoparticles against multidrug-resistant *Pseudomonas aeruginosa* biofilms. *J Proteome Res*. 2020;19:3109–3122. doi:10.1021/acs.jproteome.0c00114
45. Wang XP, Liu CX, Li HQ, et al. MetabonomicsAssisted label-free quantitative proteomics and transcriptome analysis reveals novel insights into antifungal effect of graphene oxide for controlling Fusarium graminearum. *Environ Sci Nano*. 2019;6:3401–3421. doi:10.1039/C9EN00981G
46. Durmus NG, Taylor EN, Kummer KM, Webster TJ. Enhanced efficacy of superparamagnetic iron oxide nanoparticles against antibiotic-resistant biofilms in the presence of metabolites. *Adv Mater*. 2013;25:5706–5713. doi:10.1002/adma.201302627
47. Rappsilber J, Mann M, Ishihama Y. Protocol for micro-purification, enrichment, pre-fractionation and storage of peptides for proteomics using StageTips. *Nat Protoc*. 2007;2:1896–1906. doi:10.1038/nprot.2007.261
48. Kliza K, Taeumer C, Pinzuti I, et al. Internally tagged ubiquitin: a tool to identify linear polyubiquitin modified proteins by mass spectrometry. *Nat Methods*. 2017;14:504–512. doi:10.1038/nmeth.4228
49. Cox J, Matic I, Hilger M, et al. A practical guide to the MaxQuant computational platform for SILAC-based quantitative proteomics. *Nat Protocol*. 2009;4:698–705. doi:10.1038/nprot.2009.36
50. Tyanova S, Temu T, Sinitcyn P, et al. The Perseus computational platform for comprehensive analysis of (prote)omics data. *Nat Meth*. 2016;13:731–740. doi:10.1038/nmeth.3901
51. Dang TT, Pham VH, Hur SH, et al. Superior dispersion of highly reduced graphene oxide in N, N-dimethylformamide. *J Colloid Interface Sci*. 2012;376:91–96. doi:10.1016/j.jcis.2012.03.026
52. Ferrari AC, Basko DM. Raman spectroscopy as a versatile tool for studying the properties of graphene. *Nat Nanotechnol*. 2013;8:235–246. doi:10.1038/nnano.2013.46

53. Yang D, Velamakanni A, Bozoklu G, et al. Chemical analysis of graphene oxide films after heat and chemical treatments by X-ray photoelectron and Micro-Raman spectroscopy. *Carbon*. 2009;47:145–152. doi:10.1016/j.carbon.2008.09.045
54. Yang S, Zhi L, Tang K, et al. Efficient synthesis of heteroatom (N or S)-doped graphene based on ultrathin graphene oxide-porous silica sheets for oxygen reduction reactions. *Adv Funct Mater*. 2012;22:3634–3640. doi:10.1002/adfm.201200186
55. Hui L, Piao JG, Auletta J, et al. Availability of the basal planes of graphene oxide determines whether it is antibacterial. *ACS Appl Mater Interface*. 2014;6:13183–13190. doi:10.1021/am503070z
56. Zhang T, Tremblay PL. Graphene: an antibacterial agent or a promoter of bacterial proliferation? *IScience*. 2020;23:101787. doi:10.1016/j.isci.2020.101787
57. Bæk KT, Bowman L, Millership C, et al. The cell wall polymer lipoteichoic acid becomes nonessential in *Staphylococcus aureus* cells lacking the ClpX chaperone. *MBio*. 2016;7:e01228. doi:10.1128/mBio.01228-16
58. Wang QM, Peery RB, Johnson RB, et al. Identification and characterization of a monofunctional glycosyltransferase from *Staphylococcus aureus*. *J Bacteriol*. 2001;183:4779–4785. doi:10.1128/JB.183.16.4779-4785.2001
59. Hübscher J, McCallum N, Sifri CD, et al. MsrR contributes to cell surface characteristics and virulence in *Staphylococcus aureus*. *FEMS Microbiol Lett*. 2009;295:251–260.
60. Cheng AG, Missiakas D, Schneewind O. The giant protein Ebh is a determinant of *Staphylococcus aureus* cell size and complement resistance. *J Bacteriol*. 2014;196:971–981. doi:10.1128/JB.01366-13
61. Nishida S, Kurokawa K, Matsuo M, et al. Identification and characterization of amino acid residues essential for the active site of UDP-N-acetylenolpyruvylglucosamine reductase (MurB) from *Staphylococcus aureus*. *J Biol Chem*. 2006;281:1714–1724. doi:10.1074/jbc.M509277200
62. Lowe AM, Deresiewicz RL. Cloning and sequencing of *Staphylococcus aureus* murC, a gene essential for cell wall biosynthesis. *DNA Sequence*. 1999;10:19–23. doi:10.3109/10425179909033931
63. Boonsiri T, Watanabe S, Tan XE, et al. Identification and characterization of mutations responsible for the β-lactam resistance in oxacillin-susceptible mecA-positive *Staphylococcus aureus*. *Sci Rep*. 2020;10:1–22. doi:10.1038/s41598-020-73796-5
64. Miller CR, Monk JM, Szubin R, Berti AD. Rapid resistance development to three antistaphylococcal therapies in antibiotic-tolerant *Staphylococcus aureus* bacteremia. *PLoS One*. 2021;16:e0258592.
65. Pereira MP, D'Elia MA, Troczynska J, Brown ED. Duplication of teichoic acid biosynthetic genes in Staphylococcus aureus leads to functionally redundant poly (ribitol phosphate) polymerases. *J Bacteriol*. 2008;190:5642–5649. doi:10.1128/JB.00526-08
66. Imber M, Van Loi V, Reznikov S, et al. The aldehyde dehydrogenase AldA contributes to the hypochlorite defense and is redox-controlled by protein S-bacillithiolation in *Staphylococcus aureus*. *Redox Biol*. 2018;15:557–568.
67. Wozniak DJ, Tiwari KB, Soufan R, Jayaswal RK. The mcsB gene of the clpC operon is required for stress tolerance and virulence in *Staphylococcus aureus*. *Microbiology*. 2012;158:2568–2576. doi:10.1099/mic.0.060749-0
68. Maruyama A, Kumagai Y, Morikawa K, et al. Oxidative-stress-inducible qorA encodes an NADPH-dependent quinone oxidoreductase catalysing a one-electron reduction in *Staphylococcus aureus*. *Microbiology*. 2003;149:389–398. doi:10.1099/mic.0.25796-0
69. Chang W, Small DA, Toghrol F, Bentley WE. Global transcriptome analysis of *Staphylococcus aureus* response to hydrogen peroxide. *J Bacteriol*. 2006;188:1648–1659. doi:10.1128/JB.188.4.1648-1659.2006
70. Fuller JR, Vitko NP, Perkowski EF, et al. Identification of a lactate-quinone oxidoreductase in *Staphylococcus aureus* that is essential for virulence. *Front Cell Infect Microbiol*. 2011;1:19. doi:10.3389/fcimb.2011.00019
71. Bottomley AL, Kabli AF, Hurd AF, et al. *Staphylococcus aureus* DivIB is a peptidoglycan-binding protein that is required for a morphological checkpoint in cell division. *Mol Microbiol*. 2014;94:1041–1064.
72. Lewandowski T, Huang J, Fan F, et al. *Staphylococcus aureus* formyl-methionyl transferase mutants demonstrate reduced virulence factor production and pathogenicity. *Antimicrob Agents Chemother*. 2013;57:2929–2936.
73. Yee R, Feng J, Wang J, Chen J, Zhang Y. Identification of genes regulating cell death in *Staphylococcus aureus*. *Front Microbiol*. 2019;10:2199.
74. Cerca N, Brooks JL, Jefferson KK. Regulation of the intercellular adhesin locus regulator (icaR) by SarA, σB, and IcaR in *Staphylococcus aureus*. *J Bacteriol*. 2008;190:6530–6533.
75. Cosgrove K, Coutts G, Jonsson IM, et al. Catalase (KatA) and alkyl hydroperoxide reductase (AhpC) have compensatory roles in peroxide stress resistance and are required for survival, persistence, and nasal colonization in *Staphylococcus aureus*. *J Bacteriol*. 2007;189:1025–1035.
76. Lin MH, Li CC, Shu JC, et al. Exoproteome profiling reveals the involvement of the foldase PrsA in the cell surface properties and pathogenesis of *Staphylococcus aureus*. *Proteomics*. 2018;18:1700195.
77. Tajbakhsh G, Golemi-Kotra D. The dimerization interface in VraR is essential for induction of the cell wall stress response in Staphylococcus aureus: a potential druggable target. *BMC Microbiol*. 2019;19:1–9.
78. Yeo WS, Jeong B, Ullah N, et al. Ftsh sensitizes methicillin-resistant *Staphylococcus aureus* to β-lactam antibiotics by degrading YpfP, a lipoteichoic acid synthesis enzyme. *Antibiotics*. 2021;10:1198.
79. Perez-Riverol Y, Bai J, Bandla C, et al. The PRIDE database resources in 2022: a Hub for mass spectrometry-based proteomics evidences. *Nucleic Acids Res*. 2022;50(D1):D543–D552.